iMRI

Investigative Magnetic Resonance Imaging

Efficient Experimental Design for Measuring Magnetic Susceptibility of Arbitrarily Shaped Materials by MRI

Seon-ha Hwang, Seung-Kyun Lee

Department of Biomedical Engineering, Sungkyunkwan University, Suwon, Korea
Center of Neuroscience Imaging Research, Institute for Basic Science, Suwon, Korea

Original Article

Purpose: The purpose of this study is to develop a simple method to measure magnetic susceptibility of arbitrarily shaped materials through MR imaging and numerical modeling.

Materials and Methods: Our 3D printed phantom consists of a lower compartment filled with a gel (gel part) and an upper compartment for placing a susceptibility object (object part). The B_0 maps of the gel with and without the object were reconstructed from phase images obtained in a 3T MRI scanner. Then, their difference was compared with a numerically modeled B_0 map based on the geometry of the object, obtained by a separate MRI scan of the object possibly immersed in an MR-visible liquid. The susceptibility of the object was determined by a least-squares fit.

Results: A total of 18 solid and liquid samples were tested, with measured susceptibility values in the range of -12.6 to 28.28 ppm. To confirm accuracy of the method, independently obtained reference values were compared with measured susceptibility when possible. The comparison revealed that our method can determine susceptibility within approximately 5%, likely limited by the object shape modeling error.

Conclusion: The proposed gel-phantom-based susceptibility measurement may be used to effectively measure magnetic susceptibility of MR-compatible samples with an arbitrary shape, and can enable development of various MR engineering parts as well as test biological tissue specimens.

Keywords: Magnetic susceptibility; B_0 map; MR engineering

INTRODUCTION

Magnetic susceptibility represents the degree of magnetization of a material in an applied magnetic field. It is a critical material parameter in MRI because difference of magnetic susceptibility between neighboring materials causes inhomogeneity of magnetic field, that causes distortion and signal loss in MR imaging. To predict the object-induced magnetic field inhomogeneity and devise appropriate compensation strategies, magnetic susceptibility of materials must be known (1). The purpose of this study is to demonstrate a simple and efficient way to measure the magnetic susceptibility of solid or liquid materials using MRI.

There are several existing methods for measuring magnetic susceptibility by dedicated magnetometers or MRI. For the former, a SQUID (Superconducting QUantum

iMRI

Measuring Magnetic Susceptibility of Arbitrarily Shaped Materials | Seon-ha Hwang, et al.

Interference Device) based on a pair of Josephson junctions in a superconducting loop (2) sensitively measures magnetic field perturbations induced by a test object placed in an applied magnetic field. While powerful for material characterization, most SQUID-based susceptibility measurement devices require the sample material to be small; for example, a popular MPMS system (Quantum Design, USA) can only measure objects smaller than 9 mm in diameter (3). The measurement is sensitive to paramagnetic impurities such as metallic residues from cutting devices used for sample preparation. Wapler et al. revealed a method for measuring magnetic susceptibility using MRI (4). In his method, the sample shape was limited to a cylinder, and the method could not be easily extended to an arbitrarily shaped material. Neelavalli et al. (5) measured susceptibility of arbitrarily shaped objects by measuring the B_0 maps of water surrounding the object. This method, while sensitive and flexible, can suffer from significant image distortions at the voxels close to the liquid-object interface, as we show below. Also B_0 map of water may be affected by flow artifacts in the presence of scanner vibration.

The goal of this study is to demonstrate an improved method to measure the magnetic susceptibility of an object with the following beneficial features: 1) Samples can have an arbitrary shape, 2) The flow artifact is avoided by mapping B_0 of gel instead of water, 3) Scan time is efficiently used by separately optimizing gel imaging (for low-resolution B_0 mapping) and sample imaging (for high-resolution shape determination), 4) Susceptibility artifacts due to magnetic susceptibility difference between the sample and the surrounding liquid may be reduced by using approximately susceptibility-matched liquid.

MATERIALS AND METHODS

To balance imaging speed, convenience in workflow, and measurement accuracy, we tested two protocols and two phantom geometries.

Principle

The proposed method is applied to a magnetically homogeneous material. We assume that the object of interest, solid or liquid, has a uniform and small magnetic susceptibility, $\chi \ll 1$. When placed in an MRI magnet with a static field B_0, the object develops magnetization given by $M = \chi B_0/\mu_0$, wherein μ_0 is the permeability of vacuum.

This condition is satisfied by most paramagnetic and diamagnetic materials so the technique may be applied to MR-compatible material. The principle of our technique is to measure the magnetic field inhomogeneity in a nearby MR-detectable material (gel) induced by M and compare this with numerically predicted field for the given object geometry. The object's geometry can be obtained by an MRI scan of the object itself if it is MR-visible (e.g., silicone earplug); otherwise obtained by a separate MRI scan of the outside of the object after it is immersed in an MR-visible liquid. By performing a least-squares fit of the measured magnetic field to the simulated one, we can get the magnetic susceptibility of the object (5). For simplicity, we will call the magnetic field inhomogeneity map as a B_0 map.

In our process, the measured B_0 map is reconstructed from a dual-echo gradient echo (GRE) phase images of a gel. The simulated B_0 map comes from a numerical dipolar field calculation from an input object with the shape, volume and position of the measured object. This calculation defines the object as a susceptibility source and the gel as a target, and obtains the susceptibility-induced B_0 map of the target by generalized susceptibility voxel convolution implemented in MATLAB (Mathworks, USA) (6, 7). By measuring the B_0 map not in a liquid but in a gel, flow artifact may be avoided without using flow-compensating gradients; this has an advantage that the minimum echo time may be shortened for reduced dephasing. The MR-visible liquid used to image an MR-invisible object may be doped to approximately match the object's susceptibility to minimize image distortion.

Fabrication of Phantom

A cylindrical, two-part plastic container was made by a 3D printer (Dimension 1200ES, Stratasys, USA) with an ivory ABS filament. The container consists of two parts, gel and object parts. The lower, gel part of the phantom was filled with gelatin prepared as the following. We mixed 24 g gelatin powder with 300 ml distilled water using a stirrer and boiler, adjusted to the stirrer level of 250 ppm and the temperature of 200°C. After boiling, we cooled the melted gel to 50°C and added 4.5 g Germall Plus (http://www.lotioncrafter.com/liquid-germall_plus.html) for preservative. We poured the melted gel with the preservative in the gel part of the container and cooled it at room temperature overnight before storing it in a refrigerator.

For our work, two different 3D printed container designs were used called Phantom 1 and Phantom 2. In Phantom 1, the two parts of the container could not be detached

and separated by a 5 mm wall between them. The diameter of cylinder was 74 mm and the total height was 84 mm; 50 mm for the object part and 34 mm for the gel part. In Phantom 2, the object part of the container was detachable from the gel part. Specifically, the object part had a stepped profile at the bottom, to enable its snug insertion into the lip at the top of the gel container. Figure 1 shows the picture of this phantom. Multiple detachable object parts of the container were 3D-printed for quick switching of different samples to be measured. This was particularly beneficial when the object had to be imaged, after B_0 mapping, with an MR-visible liquid filled in the container; preparation of the next object to be tested did not need to wait for washing of the whole container. Also, since the gel part does not need to move, the B_0 map of the gel without the object needs to be measured only once when testing multiple objects.

To provide a flat surface to mount the phantom on the curved head coil housing, a custom-designed mechanical supporter for the phantom was made by 3D printing (Fig. 1).

MR Imaging Acquisition

A 3T human scanner (Magnetom Prisma, Siemens Healthineers, Germany) with the posterior half of a 20-channel head-neck coil was used for all experiments. To pour the liquid before the third (object shape) imaging, the anterior half of the coil was not used. The B_0 maps were obtained from a 2D coronal-plane double-echo gradient echo sequence. The object scans also used this 2D coronal-plane sequence without slice gap to cover the whole object volume.

To find a balance between ease of data processing and efficiency of scan acquisition, two different scan protocols were tested. In the first protocol, the whole phantom, including the gel and the object compartments, was imaged in a field of view (FOV) at a moderate spatial resolution of 0.625×0.625 (in-plane) $\times 1$ (slice) mm^3. This protocol will be called a "single FOV protocol". In the second, the gel and the object parts of the phantom were scanned separately with different scan parameters. In particular, the B_0 map
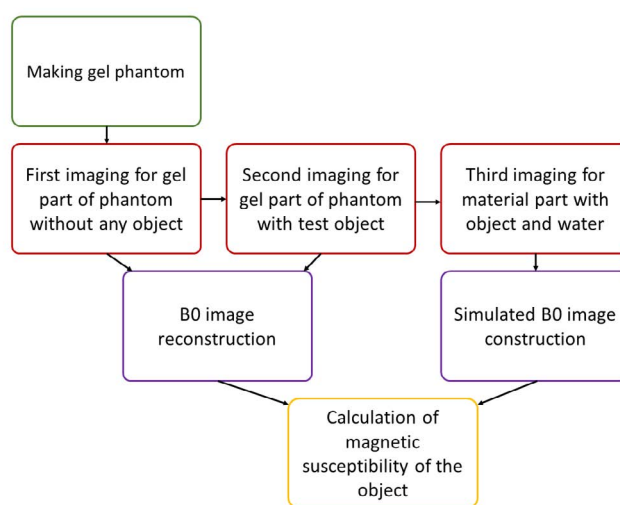

Fig. 2. Illustration of the workflow of the method to measure magnetic susceptibility by MRI.
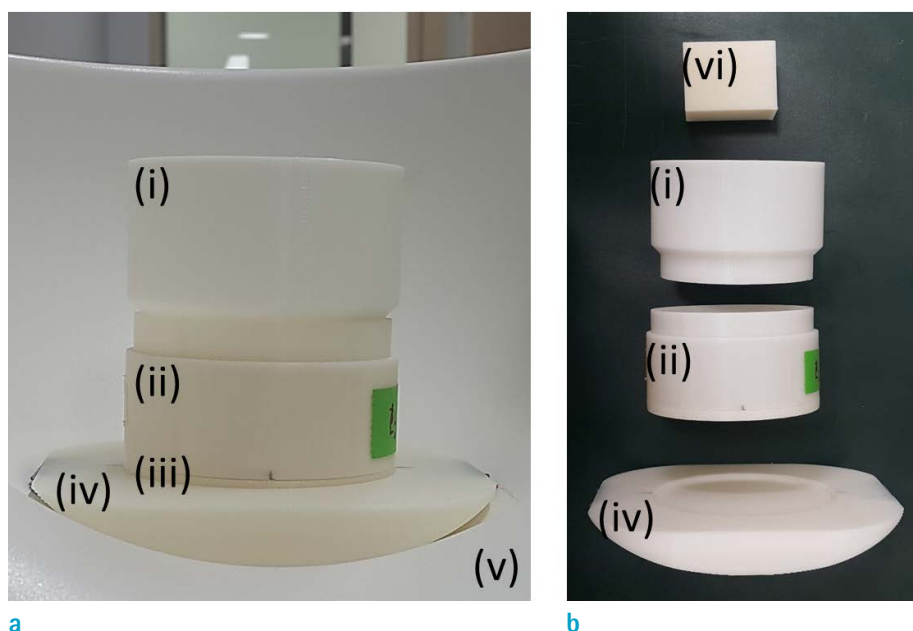

a

b

Fig. 1. (a, b) Pictures of the phantom. The phantom consists of an object part (i), gel part (ii), cap for the gel part (iii), supporter (iv), and the object (vi), and is placed in the posterior half of a head coil (v). The gel part and the object part can be detached as shown in (b).

iMRI

Measuring Magnetic Susceptibility of Arbitrarily Shaped Materials | Seon-ha Hwang, et al.

of gel was obtained with a relatively low resolution, at $2 \times 2 \times 2$ mm^3, while the object part was scanned at $0.5 \times 0.5 \times 0.5$ mm^3. The latter, high- resolution scan allowed more accurate determination of the object's geometry while keeping the total scan time reasonably short. This protocol will be called a "separated FOV protocol".

In the single FOV protocol, the B_0 map and object shape scans used the following parameters: TR = 50 ms, TE = 5.09/10.0 ms, bandwidth = 300 Hz/pixel, flip angle = 25°, acceleration factor = 2, FOV = $75 \times 120 \times 72$ mm^3. In the separated FOV protocol, the scans were obtained using the same parameters except for compartment-specific spatial resolutions (2 mm vs. 0.5 mm as explained above) and a flip angle of 35° better suited to the T1 of the gel. FOV of this protocol is $128 \times 128 \times 32$ mm^3 for the first and second images and $128 \times 128 \times 52$ mm^3 for the third image. The scan times are 12 minutes 48 seconds and 12 minutes 15 seconds respectively for single and separated FOV protocols. The scan time of separated FOV protocol will be more effective if the resolution required for the object is high.

Workflow

Our procedure is based on three imaging scans of the phantom as illustrated in the flowchart of Figure 2. First, the B_0 map of the gel is obtained without the object in the top compartment through a double-echo gradient echo scan (First Imaging). Then the object to be measured is put in place and the B_0 map of the gel, influenced by the object, is obtained again (Second Imaging). Last, an imaging liquid (tap water or gadolinium doped water) is poured in the top compartment to immerse the object and this part of the phantom is imaged to determine position and shape of

the object (Third Imaging). For an MR-visible object (such as silicone or liquid sample) no additional liquid is needed. The only difference between the single and separated FOV protocols is that the single FOV protocol set the FOV to cover the whole phantom for all three imaging scans while the separated FOV protocol used FOV covering only the gel part in the first and second scans and the object part of the phantom in the third scan.

This workflow was applied to the undetached phantom (Phantom 1) using the single-FOV protocol on the following objects: silicone earplug (McKeon Products, USA); black (high and low density) and ivory (high density) ABS cuboid blocks from a 3D printer (Dimension 1200ES, Stratasys, USA); grey (high and low density), white (high density) PLA and grey tough PLA cuboid blocks from another 3D printer (Replicator+, Makerbot, USA); and solid cylindrical pieces of Teflon, nylon and acryl.

The same workflow and scan protocol were also applied to the detachable phantom (Phantom 2), introduced to expedite the scan workflow for multiple objects, on the following samples: ivory cuboid block from the Strarasys 3D printer, and deionized water.

Figure 3 shows images from the separated FOV scan protocol applied to the detachable phantom used on an ivory cuboid block from the Strarasys 3D printer. The figure illustrates separate scans for the gel part (Fig. 3b, magnitude image from a B_0 scan) and the object part with water (Fig. 3a), and post-processing combination of the two images (Fig. 3c). As mentioned, separated gel- and object scans allowed individual optimization of the B_0 map and morphology scans, taking advantage of the fact that we do not need a high resolution in gel B_0 map scans. By this process, we
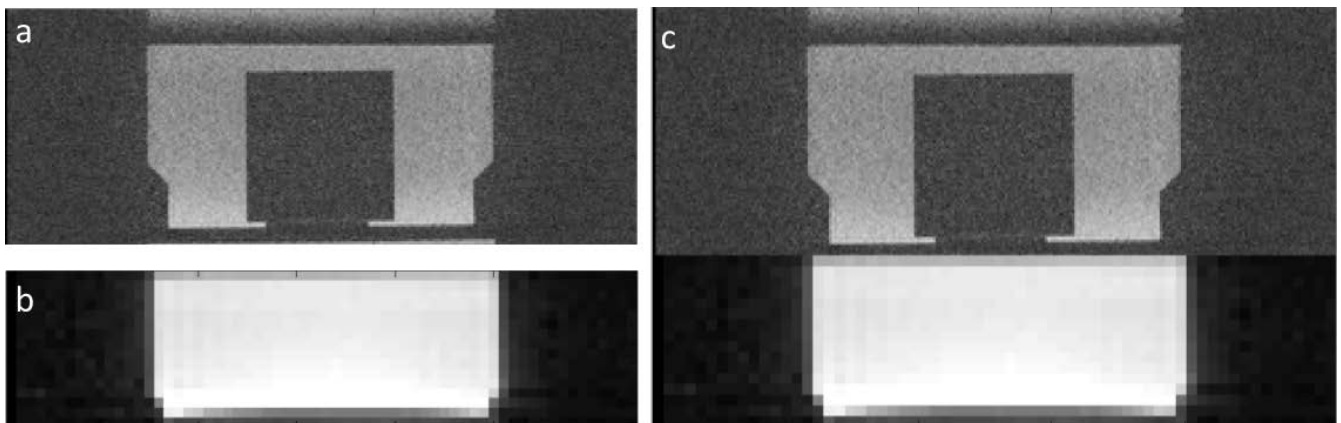

Fig. 3. Images of the object part (a) and the gel part (b) of the phantom, and their combination obtained by post-processing (c). (a) and (b) correspond to the third and the first images, respectively, on the transverse plane.

reduced the total scan time while obtaining more accurate volume and position of the imaged objects in the upper part of the phantom (50 minutes to 12 minutes). The following samples were tested using the separated FOV imaging: ivory cuboid block from the Strarasys 3D printer, an abalone shell, cuboid blocks of aluminum and copper alloys, a piece of cow bone, aqueous solution of gadolinium contrast agent (Dotarem, Guerbet, USA), distilled water, MR-compatible surgical ceramic screws (Thomas Recording, Germany). Note that objects with more random shapes and finer spatial details (abalone shell, cow bone, ceramic screws) could be tested more easily in this protocol.

High Susceptibility Objects

In determining the shape and volume of the object by imaging the surrounding liquid, one can control the susceptibility difference between the object and the liquid by appropriate choice of the liquid with known susceptibility. For example, Gd-DOTA solution has a theoretical susceptibility-per-concentration calibration (0.335 ppm/mM) (8). This may be used to reduce image distortion around objects with relatively large paramagnetic susceptibility, e.g., >20 ppm for certain PLA materials used in 3D printing. Use of a paramagnetic liquid will increase B_0 variation near the air-phantom interface, slowly varying in space. Such B_0 variation is relatively benign since the liquid is used only for shape determination of the MR-invisible object in magnitude (as opposed to phase) images in our method.

However, in cases of metal such as aluminum and copper, Gd-DOTA solution was not sufficient to eliminate artifacts. Therefore, prior shape information (cuboid) of aluminum and copper was used for more accurate modeling.

Liquid Sample

For liquid samples such as water and gadolinium solutions, a stand-alone tube or a beaker may be used for convenience of handling. In the first imaging (Fig. 2), an empty tube is taped to the bottom of the object compartment. Then an identical tube containing a liquid sample replaces the empty tube and second imaging takes place. In the third, shape-determining imaging, additional liquid is not needed because liquid samples used had MR signals.

Post-Processing

As shown in Figure 2, phase images for two echo times of the gel part are obtained in the first and second imaging. By taking the difference of the phase images at the two echo times, we get two B_0 maps of the gel with and without the object. Taking the difference of these two B_0 maps reconstructs a B_0 map that is only influenced by the object. This measured B_0 map is called B_{0m}.

From the third imaging, by taking the voxels with relatively high (low) signal in the case of MR-visible (invisible) materials, information about shape, volume, and position of the object under test is extracted. With the object's geometry information obtained, a B_0 map due to the object is calculated assuming a fixed susceptibility of the object by forward dipolar field calculation (7). This simulated B_0 map is called B_{0s}.

By comparing B_{0s} and B_{0m}, magnetic susceptibility of the material can be obtained because the object-induced magnetic field is proportional to magnetic susceptibility of the material. The value obtained from this post-processing is the relative magnetic susceptibility of the object with respect to the background material, air. Therefore, we
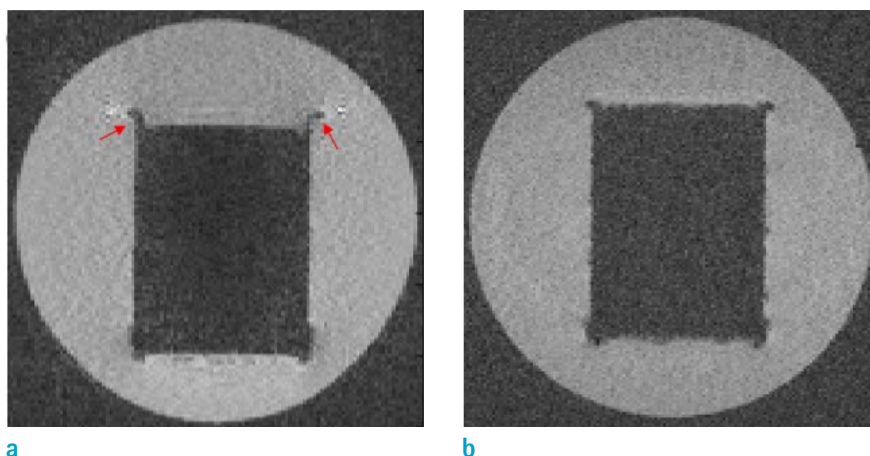

a   b

Fig. 4. Reduction of susceptibility artifacts on the object immersed in paramagnetic Gadolinium solution. (a) Magnitude image of a grey 3D printing material in tap water. (b) Magnitude image of the same material in a gadolinium solution (χ = 8.54 ppm). Red arrows indicate signal loss artifacts. Images are shown on a coronal plane.

iMRI

Measuring Magnetic Susceptibility of Arbitrarily Shaped Materials | Seon-ha Hwang, et al.

perform air susceptibility correction by adding magnetic susceptibility of air (0.36 ppm) (1) to find the absolute magnetic susceptibility of the material of interest.

The details of the post-processing can be found in the MATLAB codes shared through: https://www.mathworks.com/matlabcentral/fileexchange/.

RESULTS

Table 1 summarizes the result of magnetic susceptibility measurement. All values include air susceptibility correction. In case of water, it was measured with two different scan protocols (single FOV and separated FOV) to check reproducibility (Table 1c). Comparing measured magnetic susceptibility and reference data reveals 1.5% and 4.3% errors for single and separated FOV protocols, respectively.

The magnetic susceptibility of the silicone earplug was independently measured by a SQUID susceptometer (MPMS, Quantum Design, USA) (Table 1c). The SQUID measurement gave a magnetic susceptibility of -8.7 ppm, that agreed with our result within 3%. We suspect that a main source of error comes from the uncertainty in volume determination based on MRI.

At the time of the measurement, the exact composition of the aluminum alloy and copper alloy was unknown because they were general purpose off-the-shelf commodity materials. Therefore, results illustrate that our method can measure the magnetic susceptibility of a weakly magnetic metal.

Table 1 shows that different materials used for 3D printing have a range of magnetic susceptibilities. Specifically, a high-density grey material (PLA) from Makerbot exhibited χ = 28 ppm that can significantly degrade MR image quality if used close to an object or tissue with water-like (-9 ppm) diamagnetic susceptibility. As shown in Figure 4a, in the case of an object with such high magnetic susceptibility, signal losses occur adjacent to the object edge. After susceptibility difference mitigation with gadolinium doped solution, the signal loss is reduced as shown in Figure 4.

Figure 5 shows examples of measured (Fig. 5a, b) and simulated (Fig. 5c, d) B_0 maps of the gel due to test objects (ivory cuboid and ceramic screws). Simulated B_0 maps were obtained using the fitted magnetic susceptibility of the

Table 1. (a) Magnetic susceptibility of several materials measured by the proposed method. (b, c) Comparison between the reference and measured values

(a)

		Magnetic susceptibility (ppm)		Magnetic susceptibility (ppm)
**Silicone Earplug		-8.44	Teflon	-7.11
Strarasys 3D printer	Black (high density)	-6.96	Nylon	-8.52
	Black (low density)	-2.28	Acryl	-9.23
	Ivory (high density)	-5.78	Abalone Shell	-2.61
Makerbot 3D printer	Grey (high density)	28.28	*Aluminum Alloy	17.12
	Grey (low density)	7.64	*Copper Alloy	6.65
	White (high density)	-7.44	Cow Bone	-9.81
	New Grey (tough PLA)	-3.99	**Gadolinium	0.319 (/mM)
**Water		-8.9	Ceramic Screw	-12.60

(b)

	Phantom1+single FOV protocol (ppm)	SQUID measurement (ppm)	Difference
Silicone Earplug	-8.44	-8.7	2.7%

(c)

	Reference value	Phantom2+single FOV protocol (error)	Phantom2+separated FOV protocol (error)
Water (ppm)	-9.04	-8.9 (1.5%)	-8.65 (4.3%)

*Aluminum and copper were not pure materials but off-the-shelf alloys. **Materials for which we had reference values.

iMRI

object. Difference maps in Figure 5e and f indicate good agreement between measured and modeled B_0 distributions in the gel albeit minimal differences likely due to errors in object position determination.

DISCUSSION

Error Treatment

Table 1b and c indicate that a typical susceptibility error in our measurements is below 5%. This is likely caused by position and volume error of the tested object, determined by MRI. Because of the finite scan resolution and random noise, accuracy of volume determination is limited. By comparison of an independently measured volume (by immersion in liquid and physical measurement) and model volume measured by voxel counting, it was revealed that errors of MR-based volume measurement could be approximately 4%. The smaller the material is, the larger the relative volume error can be if the same scan resolution is used. The separated FOV protocol allows scan parameter optimization for object geometry determination independently from potentially more time-consuming B_0 map scans. In this process, therefore, the volume and position error could be reduced by choosing higher scan resolution parameters.

A disadvantage of the separated FOV protocol is potential alignment error in image combining process. For accurate numerical calculation of B_0 in the gel from the object, relative position of the object with respect of the gel should be accurately known in all three dimensions. It was assumed that the direction of the main magnetic field was exactly on the coronal imaging plane. In our measurement limited scan resolution and possibility of slightly tilted positioning of the phantom could lead to image alignment errors of 0.5 mm to 1 mm. A numerical calculation (not shown) indicated that, such error could result in up to 5% difference in measured magnetic susceptibility. Therefore this error also cannot be ignored.

Accuracy

To assess the accuracy of the MRI measurement method, SQUID susceptometry data was obtained and compared with our result on the silicone earplug material; the comparison revealed a difference of 2.7% (Table 1b). For distilled water at room temperature, there was 1.7% difference between the measured (-8.9 ppm) and the literature value (-9.05 ppm) (1) in case of the single FOV protocol. In this example, the separated FOV protocol produced higher error (4.4%) compared to the literature value due likely to image alignment error. Overall, the comparison revealed that our method gives magnetic susceptibility of the materials of interest with an accuracy of 5%, that corresponds to 0.45 ppm for a water-like susceptibility.
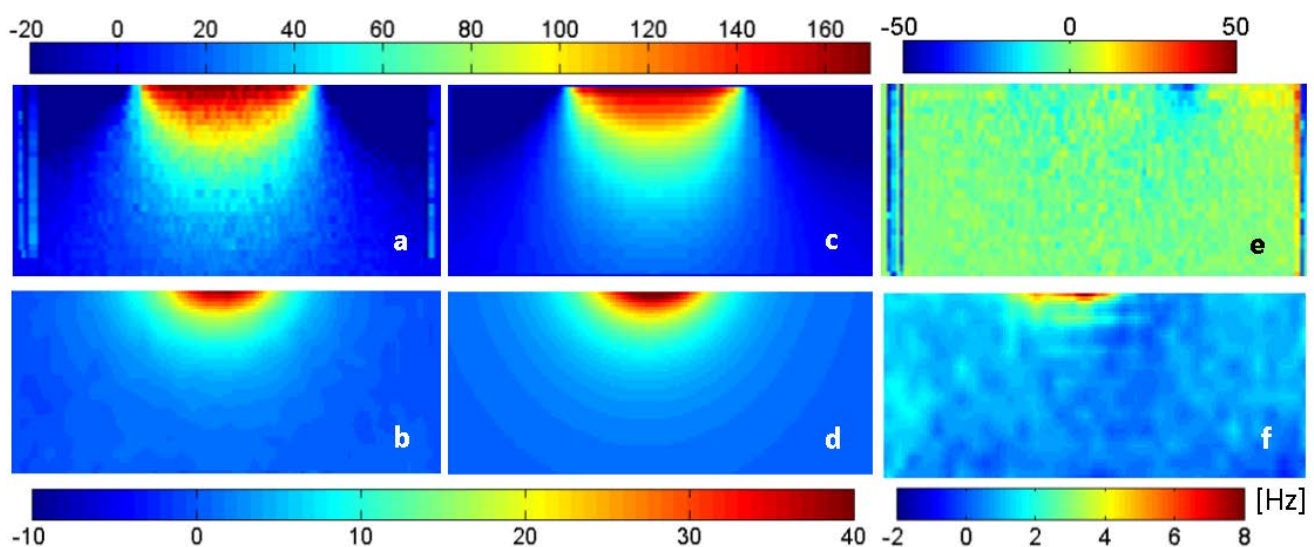

Fig. 5. B0 map comparison: measured B0 maps (a, b), simulated B0 maps (c, d), and error (= simulated minus measured) maps (e, f). Note differences in color scales. (a, c, e) are from the ivory cuboid sample and (b, d, f) are from ceramic screws which had fine features.

iMRI

Measuring Magnetic Susceptibility of Arbitrarily Shaped Materials | Seon-ha Hwang, et al.

In case of the gadolinium (Gd-DOTA) solution, measured magnetic susceptibility agreed reasonably well with literature value. Based on measurement of five different gadolinium solutions (0, 3.652, 7.25, 14.5, 29 mM), we obtained normalized magnetic susceptibility of Gd of 0.319 ppm/mM. This represents a 4.8% error compared to literature value of 0.335 ppm/mM (8).

For objects with fine features such as an abalone shell and ceramic screws, the 0.5 mm isotropic resolution may be insufficient to reconstruct the object's morphology with full details. Therefore, measuring accurate magnetic susceptibility in such objects can be limited by object modeling errors. One mitigation strategy would be to use prior knowledge about the object's total volume, determined independently by physical measurements. Then, the intensity threshold for defining the object's shape mask from the third imaging can be adjusted to match the measured volume. This way a large scale (lowest order) modeling error can be minimized.

Reduction of Susceptibility Artifacts in Liquid-filled Scan

In case of the gray cuboid from Makerbot 3D printer and the aluminum and copper alloys, there were artifacts around the material in the third images when water was used as the filling liquid. This is suspected to be partly due to relatively large difference of the magnetic susceptibility between the object and background water (9, 10). To reduce the mismatch, Gd-DOTA solution with estimated susceptibility of 8.5 ppm was used instead of water in the third imaging for the grey cuboid. Note that the object-liquid susceptibility matching does not have to be exact as our purpose is to reduce the gross mismatch and avoid severe artifacts. In our case, the susceptibility of the Gd solution was determined based on a preliminary measurement with material immersed in tap water. As shown in Figure 4, it reduced the signal losses around the object especially near the corners. In metals, however, artifacts were not significantly removed even though susceptibility-matching between the liquid and object was better than for the grey material.

In the case of metallic materials, RF eddy current would cause RF field distortions near the object. Therefore, we suspect that artifacts for the highly conductive metal pieces were contributed more by B_1 than B_0 map distortion, that needs further investigation. For artifact-reduced imaging of metallic objects, recent published methods could be considered in the future (11).

Comparison with Previous Methods

The main difference of our method compared with the previous methods (4, 5) is that B_0 map scan and object shape scan can be performed independently. This is possible by taking the B_0 map in a gel in a different container than the susceptibility source object. The remote gel imaging strategy also removes flow artifacts in phase-based B_0 mapping. Separate shape determination scan permits more flexibility in imaging high magnetic susceptibility materials and possibly metallic objects. For example, in the case of the grey cuboid, using paramagnetic gadolinium-doped solution (52 mM for 8.5 ppm total susceptibility) instead of water as a filling liquid significantly reduced susceptibility artifacts in the object's shape determination while not affecting B_0 mapping in the gel. If the method of Neelavalli et al. (5) were to be used with similar susceptibility artifact mitigation, B_0 maps would have to be determined by phase imaging of the Gd-doped water, which would have a poor SNR due to strong R2* relaxation (12). Therefore, in our method, more materials can be measurable compared to the other methods.

In conclusion, we demonstrated an efficient and practical method for measuring magnetic susceptibility of a weakly magnetic, arbitrarily shaped object. The method can be used for characterization of a wide range of MR-compatible materials in MR engineering.

REFERENCES

1. Schenck JF. The role of magnetic susceptibility in magnetic resonance imaging: MRI magnetic compatibility of the first and second kinds. Med Phys 1996;23:815-850
2. Schwartz B. Superconductor applications: SQUIDs and machines. Springer Science & Business Media New York: Springer US, 2013
3. MPMS 3 Product Description; Available from: https://www.qdusa.com/sitedocs/productBrochures/1500-102.pdf. Accessed September 8, 2018
4. Wapler MC, Leupold J, Dragonu I, von Elverfeld D, Zaitsev M, Wallrabe U. Magnetic properties of materials for

MR engineering, micro-MR and beyond. J Magn Reson 2014;242:233-242

5. Neelavalli J, Cheng YC, Haacke EM. A fast and robust method for quantifying magnetic susceptibility of arbitrarily shaped objects using MR. Proc Intl Soc Mag Reson Med 2008;16:3056

6. Yoder DA, Zhao Y, Paschal CB, Fitzpatrick JM. MRI simulator with object-specific field map calculations. Magn Reson Imaging 2004;22:315-328

7. Lee SK, Hwang SH, Barg JS, Yeo SJ. Rapid, theoretically artifact-free calculation of static magnetic field induced by voxelated susceptibility distribution in an arbitrary volume of interest. Magn Reson Med 2018;80:2109-2121

8. Chu SC, Xu Y, Balschi JA, Springer CS Jr. Bulk magnetic susceptibility shifts in NMR studies of compartmentalized samples: use of paramagnetic reagents. Magn Reson Med 1990;13:239-262

9. Joe E, Ghim MO, Ha Y, Kim DH. Accurate localization of metal electrodes using magnetic resonance imaging. J Korean Soc Magn Reson Med 2011;15:11-21

10. Czervionke LF, Daniels DL, Wehrli FW, et al. Magnetic susceptibility artifacts in gradient-recalled echo MR imaging. AJNR Am J Neuroradiol 1988;9:1149-1155

11. Astary GW, Peprah MK, Fisher CR, et al. MR measurement of alloy magnetic susceptibility: towards developing tissue-susceptibility matched metals. J Magn Reson 2013;233:49-55

12. Park SH, Nam Y, Choi HS, Woo ST. Quantification of gadolinium concentration using GRE and UTE sequences. Investig Magn Reson Imaging 2017;21:171-176